 Bull. Chem. Soc. Jpn. Vol. 84, No. 4, 427–436 (2011)

Highly Efficient Photoinduced Electron Transfer in a Novel Tetrakis(tetraphenylporphyrinatozinc)/Perylenetetracarboxidiimide Array and Its Application to a Photovoltaic Device

Fuling Wang,[1,2] Jianguo Tang,*[1,2] Jixian Liu,[1,2] Yao Wang,[1,2] Rui Wang,[1,2] Lin Niu,[1,2] Linjun Huang,[1,2] and Zhen Huang[1,2]

[1]Institute of Hybrid Materials, Laboratory of New Fiber Materials and Modern Textile, The Growing Base for State Key Laboratory, Qingdao University, Qingdao 266071, P. R. China

[2]Department of Materials Science and Engineering, College of Chemistry, Chemical and Environmental Engineering, Qingdao University, Qingdao 266071, P. R. China

Received November 1, 2010; E-mail: jianguotangde@hotmail.com

A novel donor–acceptor array consisting of four 5-(*p*-substituted phenyl)-10,15,20-triphenylporphyrinatozinc (POR) complexes attached to the 1,6,7,12-positions of perylene-3,4:9,10-tetracarboxidiimide (PDI) was synthesized and characterized. HOMO and LUMO values of the array were aquired by cyclic voltammetry. Photophysical properties were studied by steady-state UV–vis and fluorescence spectroscopy. The results showed that this compound absorbs strongly from 300 to 700 nm, making it an ideal system to harvest polychromatic light. After selective excitation of the POR moiety or PDI moiety, an almost complete fluorescence quenching was observed, indicating that highly efficient photoinduced electron transfer occurs in this array. The predominant quenching process for PDI–POR_4 array is electron-transfer yielding POR_4^+–PDI^-. The self-assemblies of this molecular in polar and nonpolar solvents were investigated. Intermolecular π–π interaction in cooperation with the van der Waals interaction between POR and PDI component leads to the formation of spherical nanoparticles and ribbon-like morphological structures in methanol and *n*-hexane, respectively. Photoelectrochemical studies exhibited prompt and steady photocurrent photovoltage response. Moreover, photovoltaic measurement on this array reveals efficient light energy conversion properties, such as a fill factor of 0.42. These results are of particular relevance for photovoltaic nanodevices and solar energy conversion applications.

Electron-transfer and energy-transfer processes between a donor and an acceptor play a fundamental role in applications such as solar cells and basic biological photosynthesis. Therefore, there is considerable interest in the design of systems composed of electron donor and acceptor entities. In particular, self-assemblies of functional molecular materials with large conjugated electronic structures into well-defined nanostructures depending on various noncovalent interactions have attracted increasing research interests in both material and chemistry fields.[1–6] Such organized assemblies make it possible to show the new phenomena and properties in comparison with those of corresponding monomeric forms.[7–13]

Recently, we have prepared synthetic architectures that perform functions such as light harvesting and photocurrent generation. Porphyrins contain an extensively conjugated two-dimensional π-system, which provides both strong absorption in the visible region and redox features that make these architectures specially suitable for photoinduced charge separation.[14–18] On the other hand, many designs for light harvesting and molecules include perylenediimides either as the core entity or as part of the antenna.[19–23] This is due to both photochemical and chemical stability of perylenediimides and straightforward functionalization of the parent structure at imide positions and more recently at the bay region. Perylene absorbs strongly in the trough between the Soret band and the Q-band of the porphyrin, thereby complementing the weak absorption of the porphyrin in this spectral region. Thus, both porphyrins and perylenediimides are promising major building blocks for superstructures.[24–28]

There are numerous reports on the self-assembly of both zinc porphyrin and PDI derivatives alone, yet there are relatively few examples in which both of these important donor–acceptor building blocks are incorporated into specific covalent structures to elicit different supramolecular photofunctional assemblies.[29–31] Here we wish to describe a novel, covalently linked array **1** (Figure 1) constructed from four 5-(*p*-substituted phenyl)-10,15,20-triphenylporphyrinatozinc (POR) complexes attached to the 1,6,7,12-positions of perylene-3,4:9,10-tetracarboxidiimide (PDI). It was characterized by ^{1}H NMR, elemental analysis, and FT-IR measurements. In addition, we report the fabrication and characterization of a photovoltaic device based on PDI–POR_4 (molecule **1**) assembly. We hope that these new designed donor–acceptor molecules could be of importance for future studies on organic materials applied to photovoltaic devices.

Experimental

Materials. Unless otherwise stated, all reagents and solvents were commercially obtained and used as received. 5-(*p*-Hydroxyphenyl)-10,15,20-triphenylporphyrin (**5**) was synthesized according to the literature.[32]

Published on the web April 7, 2011; doi:10.1246/bcsj.20100305

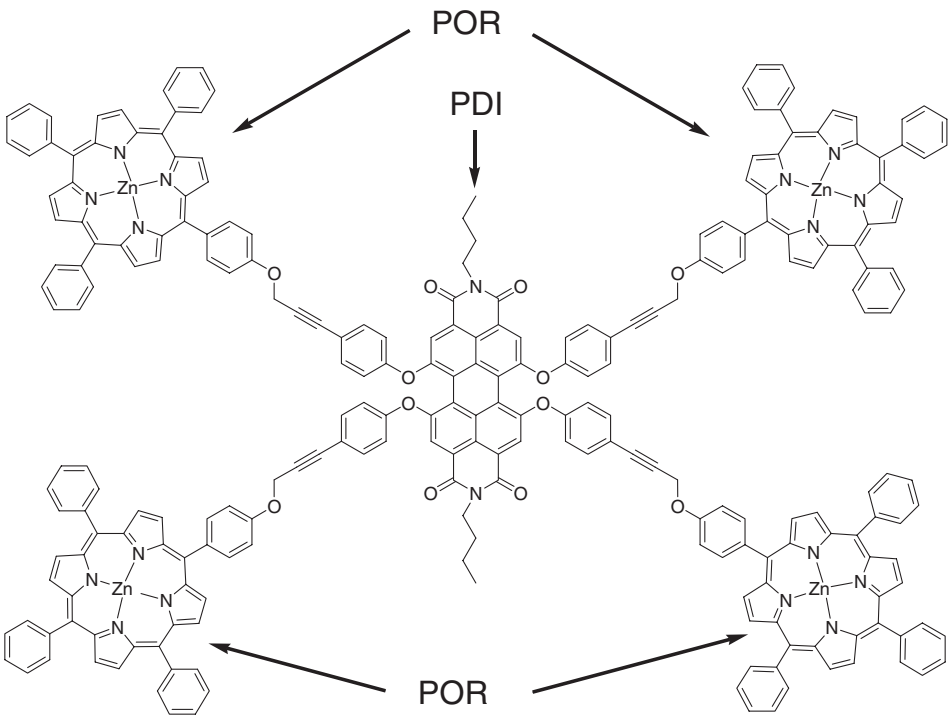

Figure 1. Structure of array **1**, PDI–POR_4.

Characterization and Measurements. UV–vis spectra were measured on a UV755B spectrometer. Fluorescence spectra were recorded on a Shimadzu RF-5310PC spectrometer. FT-IR spectra were recorded on a Nicolet 5700 FT-IR spectrometer with KBr pellets. ^{1}H NMR (600 MHz) spectra were recorded on a JNM-ECP600 spectrometer. Chemical shifts (δ values) are given in parts per million with tetramethylsilane as an internal standard. Elemental analyses were carried out on a Vario ELIII elemental analyzer. Time-resolved fluorescence measurements were performed using an ISSK2 multifrequency and phase modulation spectrofluorometer. Lifetimes were obtained on samples that had concentration of 0.5–10 μM and were deaerated by bubbling with N_2. Modulation frequencies from 20 to 300 MHz were utilized, and both the fluorescence phase shift and modulation amplitude were analyzed. The X-ray diffraction (XRD) data were collected with a Bruker D-8 X-ray diffraction meter using Cu Kα radiation ($\lambda = 0.154$ nm). XPS (X-ray photoelectron spectroscopy) measurements were collected on a ThermoFisher ESCAlab 250 X-ray photoelectron spectrometer with Al Kα monochromatized radiation as an excitation source. Surveys and high-resolution spectra were recorded with an Advantage processing program provided by ThermoFisher Scientific.

Cyclic voltammetry (CV) was conducted on a CHI760C voltammetric analyzer with glassy carbon microelectrode, Pt wire, and $Ag/AgNO_3$ electrode as working electrode, counter electrode, and reference electrode, respectively, in a 0.1 M tetrabutylammonium (TBAP) chloroform solution. Each measurement was calibrated with ferrocene (Fc),[33] with the measured $E^{Fc}_{1/2} = -0.172$ V vs. $Ag/AgNO_3$. Oxidation and reduction potentials were obtained as an average value between each anodic and corresponding cathodic potential: $E^{Fc}_{1/2} = 1/2(E_{pc} + E_{pa})$. HOMO and LUMO energy levels were estimated on the basis of the reference energy level of ferrocene (4.8 eV below the vacuum level)[33] according to $E^{HOMO}/E^{LUMO} = 4.8 + (E_{1/2} - E^{Fc}_{1/2})$ eV below the vacuum level. These HOMO/LUMO values do not represent any absolute solid-state or gas-phase ionization potentials but can be used to compare different compounds relative to one another.

Scanning electron micrographs (SEM) were carried out on a JSM-6390 LV instrument. Transmission electron micrographs were recorded on a JSM-1200 EX instrument. Sample A was prepared from evaporation of a drop of array **1** (PDI–POR_4) solution in chloroform on a quartz plate. Samples B and C were fabricated by injecting a small volume of **1** solution in chloroform into a large volume of methanol and hexane, respectively. Then the solids that precipitated from methanol and *n*-hexane were transferred to a quartz substrate for analysis.

The assemblies of array **1** are assembled onto a nanostructured SnO_2 electrode (denoted as OTE/SnO_2). The deposition procedure is as follows. **1** is dissolved in a good solvent (toluene), and then the resulting toluene solution is rapidly injected into a poor solvent (acetonitrile) to form clusters derived from the lyophobic nature in the mixed solvent (acetonitrile:toluene = 5:1). Two OTE/SnO_2 electrodes were kept at a distance of 6 mm using a Telfon spacer and set in the cuvette containing the cluster solution, and then a direct current (dc) voltage (250 V) was applied for 2 min between two electrodes using a power supply (ATTA model AE-8750). The deposition of the film could be confirmed visibly as the solution became colorless. OTE/SnO_2 electrode coated with PDI–POR_4 nanoparticles is referred to as OTE/SnO_2/PDI–POR_4. Keithley 2400 was used for recording photocurrent and photovoltage responses, a PLS-SXE 300 xenon light resource was used to give a simulated irradiance of 100 mW cm^{-2} (equivalent to AM

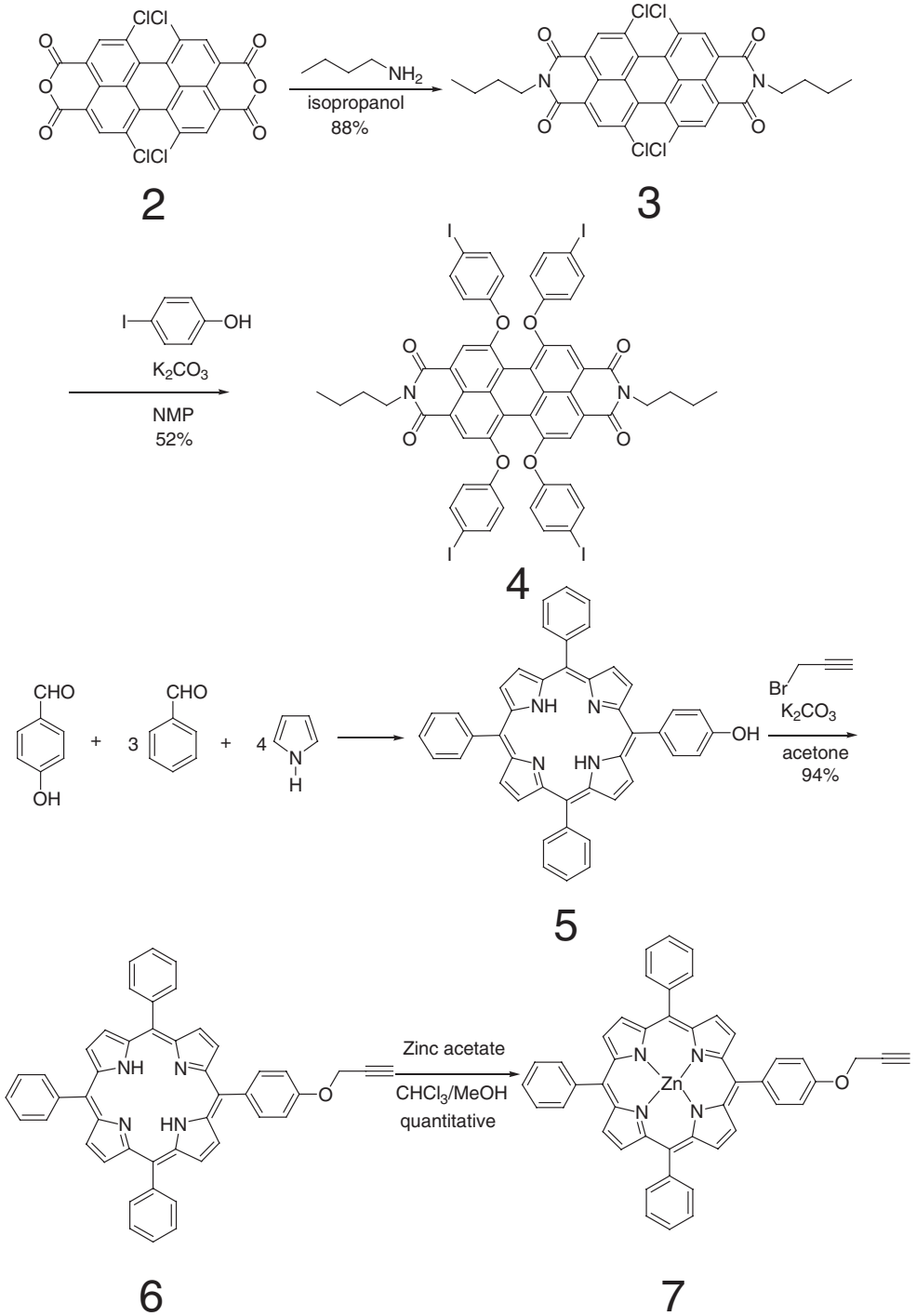

Scheme 1. Syntheses of PDI and POR fragments **4** and **7**.

1.5 irradiation) at the surface of the device. Photoelectrochemical measurements were carried out in a standard two-compartment cell consisting of a working electrode and a Pt wire gauze counter electrode in the electrolyte. The electrolyte was NaI (0.5 M) and I_2 (0.01 M) in acetonitrile. When recording a photocurrent action spectrum, the monochromatic light through a monochromator was illuminated on the modified area of the working electrode from the back side.

Syntheses. The syntheses of compounds **4**, **7** and target compound **1** are depicted in Scheme 1 and Scheme 2, respectively. The structures of array **1** and other compounds were confirmed by ^{1}H NMR spectrum, FT-IR spectra, and elemental analysis data, and related information is listed in the Supporting Information.

Results and Discussion

The absorption spectrum of the array PDI–POR_4 (**1**) in toluene with 1% pyridine is compared in Figure 2 with those of the PDI (**4**) and POR (**7**) fragments. The use of four POR units is beneficial to enhance the light-energy collection ability in the

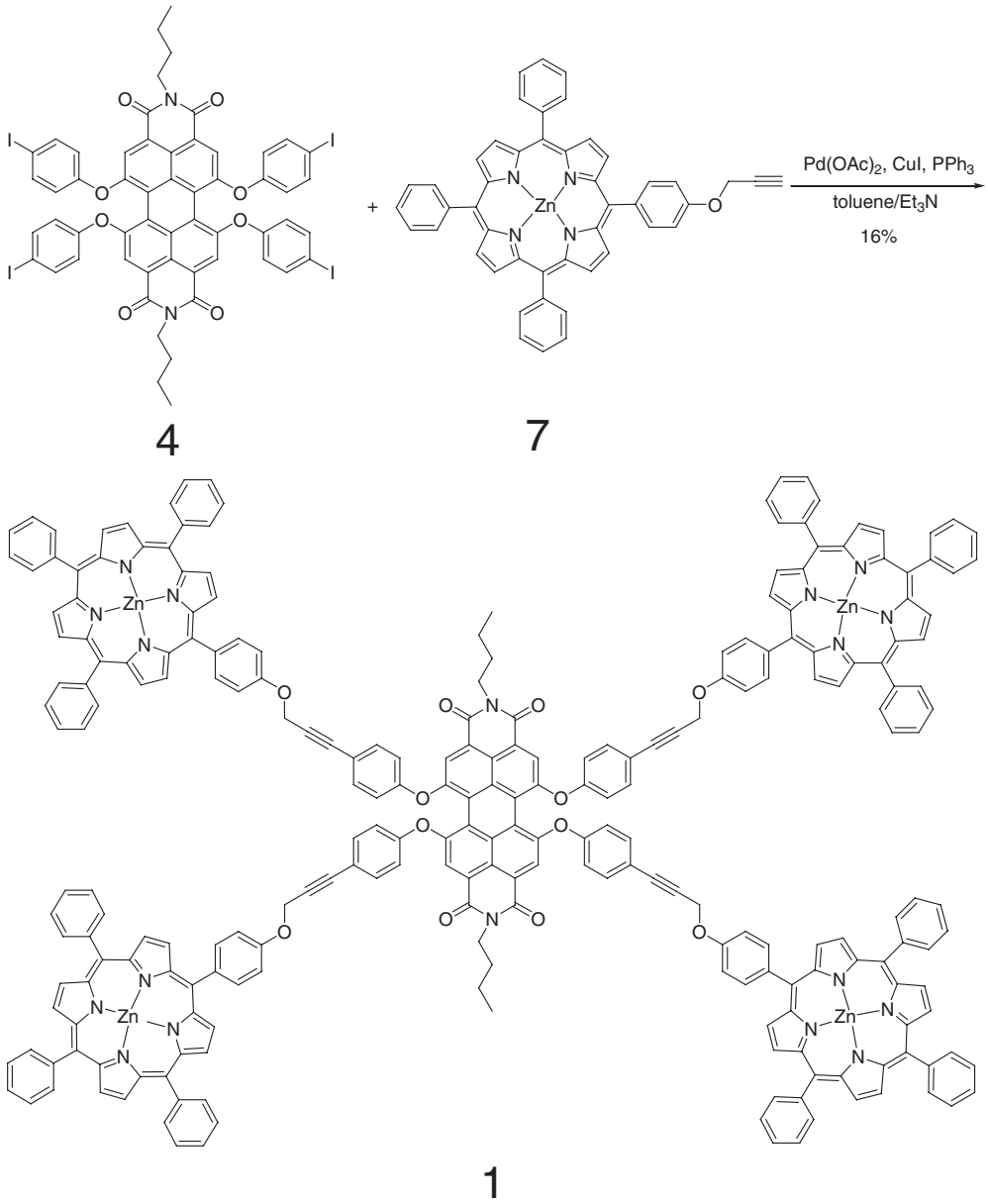

Scheme 2. Synthesis of PDI–POR_4 (**1**) using Sonogashira coupling.

region of 380–450 nm. Perylenediimide **4** exhibits its typical singlet ($S_0 \rightarrow S_1$) transition in the range of 380–620 nm ($\lambda_{max} = 560$ nm) with well-resolved vibronic structure that can be attributed to breathing vibrations of the perylene skeleton.[34] The absorption spectra of **7** contains a strong peak at 430 nm attributed to the Soret band of porphyrin, as well as a group of weak peaks at 522, 561, and 602 nm ascribed to the Q-bands of porphyrin. Thus, absorption of compounds **4** and **7** do not have considerable overlap, which makes them suitable for selective excitation studies. It can be seen that array **1** absorbs strongly from 300 to 700 nm which covers the strong radiation scope of sunlight, making it an ideal system to harvest polychromatic light. Compared to the absorption spectrum of model compound **4**, there is a slight red shift (1–3 nm) of the absorption peaks in the absorption of array **1**, this is similar to the red shift perylenediimides show upon aggregation.[35] In absorption of PDI–POR_4 there is also a slight red shift (2–5 nm) of the zinc porphyrin bands. Therefore, aside from small differences in the absorption peaks and intensities, the spectrum of the array is a good superposition of those of the molecular components, which indicates weak ground-state electronic coupling between the chromophores, and the electronic interaction between the donor (POR) and acceptor (PDI) is weak.[36,37]

The components in the array can be excited with good selectivity: at 430 nm most of the photons are absorbed by porphyrin moieties, whereas at 560 nm the perylenediimide absorbs strongly. The photoexcited state of **1** was investigated by steady-state fluorescence measurements (Figure 3). The measurements of Figure 3a were carried out at an excitation wavelength of 430 nm, where the POR moiety was exclusively excited. The measurements of Figure 3b were carried out at an excitation wavelength of 560 nm. When the POR moiety of the array **1** was excited at 430 nm, as expected, emission occurred

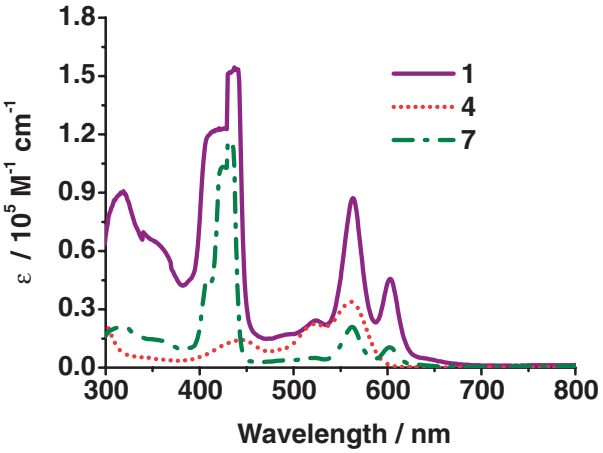

Figure 2. Absorption spectra of **1** (solid), **4** (dot), and **7** (dash dot) in toluene with 1% pyridine. Concentration = 2×10^{-5} M.

essentially exclusively from the porphyrin. However, the intensity of POR* emission in compound **1** is reduced considerably from that in the reference compound **7**. The process responsible for the effective quenching of the porphyrin excited singlet state is very likely electron transfer leading to the charge-separated product POR* (S_1) → PDI^-–POR_4^+.

Predominant excitation of the perylenediimide at 560 nm gives an emission mainly from the porphyrin chromophore (Figure 3b), this finding is indicative of substantial energy transfer from the photoexcited perylene (PDI*) to the ground state zinc porphyrin to produce the porphyrin excited-state POR*. It must be stressed that the porphyrin fluorescence in PDI–POR_4 is much weaker than of free zinc porphyrin **7**. These results reveal that energy transfer and charge separation took place via PDI* and formed POR_4*–PDI and PDI^-–POR_4^+, which can be supported by HOMO and LUMO values (see below). This significant fluorescence quenching is clearly observed, indicating that highly efficient photoinduced electron transfer occurs in this array.[37] The fluorescence quenching in multichromophoric systems has been observed in several previously reported studies.[25,37–39] As can be seen from Figure 3, the emission peak of this array is presented as two distinct peaks, and the two peaks have approximately equal heights. This phenomenon, which is a manifestation of dipole coupling of the chromophores, is quite common in multichromophoric systems and is not limited to crystalline or aggregate states,[40] as many examples in dilute solutions have been reported.[41–43] Therefore, array **1** would be most useful as an all-optical gating-element in which excited-state energy in this chromophore can be quenched by the charge-separated state of the perylene–porphyrin array, thereby shunting the light output or flow of energy.

The lifetime of the POR* excited state of array **1** was measured by fluorescence modulation (phase shift) spectroscopy. Array **1** in toluene exhibits dual-exponential fluorescence decay (λ_{ex} = 430 or 550 nm). The lifetime components are ca. 0.3 and ca. 1.6 ns with a 90/10 amplitude ratio. The shortening of the POR* lifetime to 0.3 ns for the array **1** from 2.3 ns for the reference compound **7**, is indicative of a process (such as electron transfer from POR* to the perylenediimide) that is

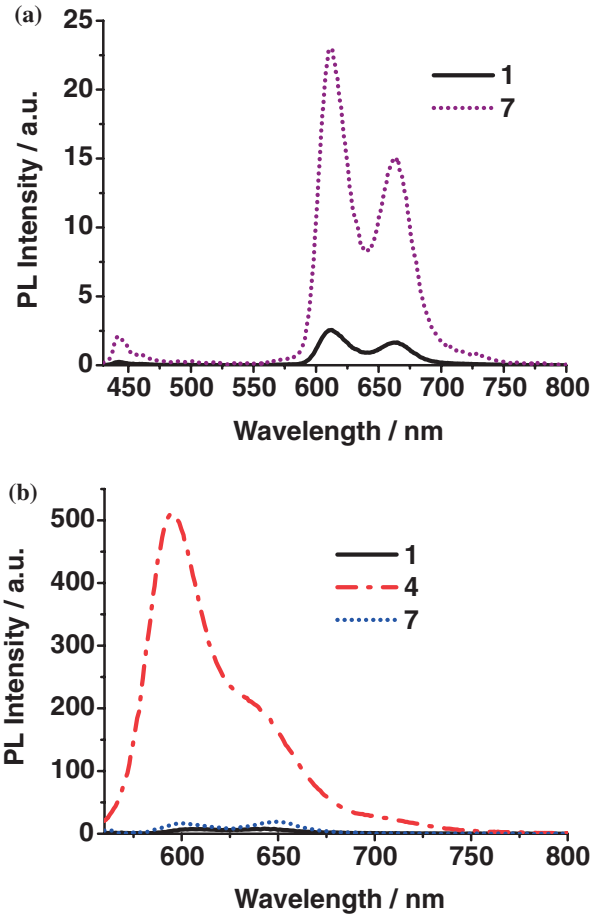

Figure 3. Fluorescence emission in toluene with 1% pyridine solutions. (a) λ_{ex} = 430 nm, **1** (solid), **7** (dot); (b) λ_{ex} = 560 nm, **1** (solid), **4** (dash dot), and **7** (dot). Concentration = 2×10^{-5} M.

not present in the reference compound. The rate constant for fluorescence quenching can be calculated from the equation[31]

$$k_q = 1/\tau_{f\,sample} - 1/\tau_{f\,reference} \quad (1)$$

where $\tau_{f\,sample}$ is the lifetime of the POR* in the array, while $\tau_{f\,reference}$ refers to the lifetime of reference sample **7**. In this context, a k_q of $2.9 \times 10^9\ s^{-1}$ was obtained, which was calculated from the fast component of the POR* emission decay (τ_f value for reference compound **7** is 2.3 ns).

To elucidate the energetic conditions for electron transfer in dilute solutions, we also determined the HOMO/LUMO values of all three compounds, **4**, **7**, and **1**, using cyclic voltammetry (CV).

All the redox potentials (V vs. Fc) and HOMO/LUMO values are given in Table 1. Donor **7** shows three oxidation peaks corresponding to 0.81, 1.12, and 1.40 V vs. Fc, which results in a HOMO value of 5.61 eV (on the basis of the HOMO energy level of ferrocene as 4.8 eV). Similarly, acceptor **4** exhibits one oxidation peak at 1.06 V vs. Fc, and two reduction peaks at −1.02 and −1.15 V vs. Fc. This gives a HOMO value of 5.86 eV and a LUMO value of 3.78 eV for compound **4**. Figure 4 exhibits the CV traces for the oxidation and reduction of PDI–POR_4 (**1**). It exhibits oxidation peaks at 0.78, 1.10, and 1.41 V vs. Fc. The three oxidation peaks are due

Table 1. Redox Potentials (V) and HOMO/LUMO Values (eV) of **4**, **7**, and **1** Measured in Solution Cyclic Voltammetry[a)]

Compound	E_{ox1}	E_{ox2}	E_{ox3}	HOMO	E_{red1}	E_{red2}	LUMO
7	0.81	1.12	1.40	5.61	−1.65		3.15
4	1.06			5.86	−1.02	−1.15	3.78
1	0.78	1.10	1.41	5.58	−0.81		3.99

a) Fc: Ferrocene and $E^{Fc}_{1/2} = -0.172$ V vs. $Ag/AgNO_3$.

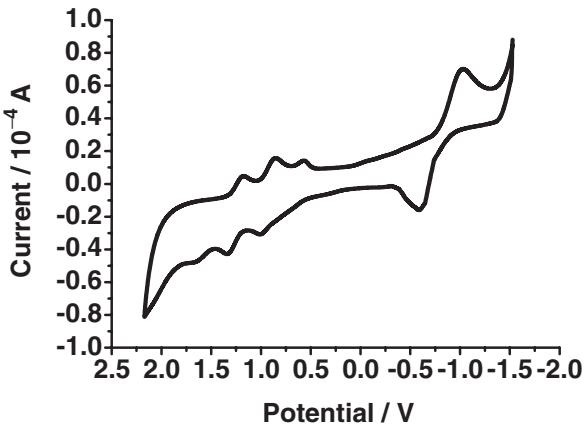

Figure 4. Cyclic voltammogram of array **1** in 0.1 M TBAP in chloroform at scan rate of 50 mV s^{-1}. The measurement was carried out at a glassy carbon microelectrode against $Ag/AgNO_3$ as the reference electrode, was calibrated with ferrocene.

to the POR moiety, in agreement with the values measured for **7** under the same conditions. The corresponding HOMO energy values determined are 5.58 eV. Additionally, the reduction peaks due to the acceptor moiety appears at −0.81 V vs. Fc. This results in a LUMO value of 3.99 eV for the acceptor unit in **1**. Therefore, the array **1** has a low band gap of 1.59 eV and a relatively low HOMO level of 5.58 eV. Thus, these energy values fulfill the energetic conditions required for the proposed electron transfer between them (from donor to acceptor on excitation of the donor as well as on direct excitation of the acceptor moiety), which could be observed as the fluorescence quenching. Figures 5a and 5b depict one of the possible channels of concurring charge-transfer processes after the direct excitation of donor at 430 nm and after the direct excitation of acceptor at 560 nm, respectively.

The morphology of the aggregates formed was examined by scanning electron microscopy (SEM) and transmission electronic microscopy (TEM). Figure 6 presents SEM and TEM images of these three samples. According to the model set up by Srinivasarao and co-workers,[44] molecular materials dissolved in a solvent with density higher than that of water usually yield two-dimensional air bubbles and a three-dimensional network, respectively, after the natural evaporation of solvent in air in the cases of lack of and existence of significant intermolecular interaction. Basically, natural evaporation of the $CHCl_3$ solution led to the formation of three-dimensional network nanostructures (Figure 6a, left), revealing the significant intermolecular interaction.[45] As can be seen from

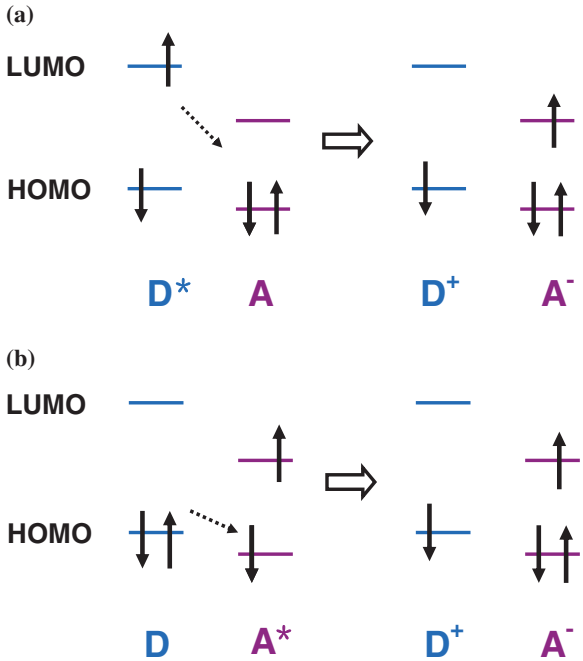

Figure 5. (a) One possible channel of electron transfer and fluorescence quenching after direct excitation of donor at 430 nm and (b) one possible channel of electron transfer and fluorescence quenching after direct excitation of acceptor at 560 nm.

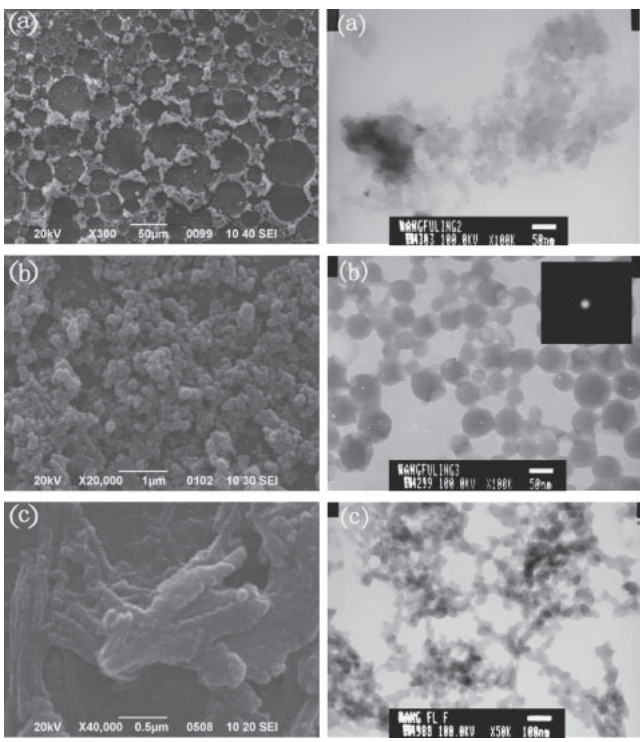

Figure 6. SEM and TEM images of array **1** aggregates. (a) Three-dimensional network nanostructures formed in $CHCl_3$ solution from sample A; (b) spherical particles formed in methanol from sample B; Inset: the electronic diffraction patterns of the array. (c) Ribbon-like structures formed in hexane from sample C.

Figure 6b (left), large amounts of spherical nanoparticles are closely packed, suggesting self-assembled nanoscale aggregates. The solids that precipitated from nonpolar solvent (hexane) however, showed an aggregated ribbon-like structure (Figure 6c, left), which manifested the solvent effect on the formation of self-assembled nanostructures of compound **1**. As can be seen from the TEM images of sample C, the ribbon-like structures were constructed from continuously connected spherical nanoparticles. It was probably caused due to the intermolecular π–π interactions in cooperation with the van der Waals interaction of the zinc porphyrin component and perylene component. It is noteworthy that the dimensional value shown in SEM was not precise because of the resolution. As shown in TEM images of samples B and C, both of the aggregates were constructed from a large quantity of nanospheres with diameters in the range of 50–100 nm. Interestingly, many concave hulls were observed clearly on the surface of these spheres. This phenomenon has previously been discovered in several other classes of compounds.[39,46] Additionally, the electronic diffraction patterns performed no elaborate crystalline diffraction pattern structures, indicating that no highly ordered crystal lattice structure was formed in these self-assembled aggregates. To further ascertain the amorphous structure, XRD patterns of array **1** together with its reference compounds **4** and **7** are shown in Figure S1 (Supporting Information). The relatively low degree of crystallinity of compound **4** may be attributed to the two butyl chains. It is found that, after the porphyrin moiety was attached to the perylene core, X-ray diffraction patterns of **1** did not show diffraction peaks that can be ascribed to the crystalline structure of porphyrin **7** and perylene **4** suggesting amorphization of the solid. Considering the elaborate crystalline structures of reference compounds **4** and **7** as evidenced by the XRD results, it can be concluded that steric hindrance was one factor that impeded the formation of crystalline structures of porphyrin and perylenediimide themselves, which leads to the final amorphous structures.

A representative survey (wide-scan) spectrum of the PDI–POR_4 (**1**) is shown in Figure 7. The XPS wide-scan spectra for reference compounds **4** and **7** are given in the Supporting Information (Figure S2). The high-resolution XPS for **1** are given in the Supporting Information (Figure S3), which shows the N 1s, C 1s, and O 1s spectra regions. As can be seen from Figure 7, the Zn $2p_{2/3}$ and Zn $2p_{1/2}$ peaks were clearly observed at 1022 and 1045 eV, repectively, in additions to the O 1s, C 1s, and N 1s peaks, which are indicative of metal-centered porphyrin moiety in array **1**.[47] After the correction of the photoelectron cross-section factors, the experimentally determined value of N:O atom ratio is consistent with the expected 3:2 stoichiometry.[48]

Compared with the corresponding dilute solution 10^{-5} M in chloroform, the UV–vis absorption spectrum of the film **1** showed much broadened and red-shifted bands (Supporting Information, Figure S4), which suggested that the π–π interactions also played an important role in formation of the film.

The nanostructures formed in PDI–POR_4 array would be promising candidates for applications in electronic devices through the combinations of π–π interactions with van der

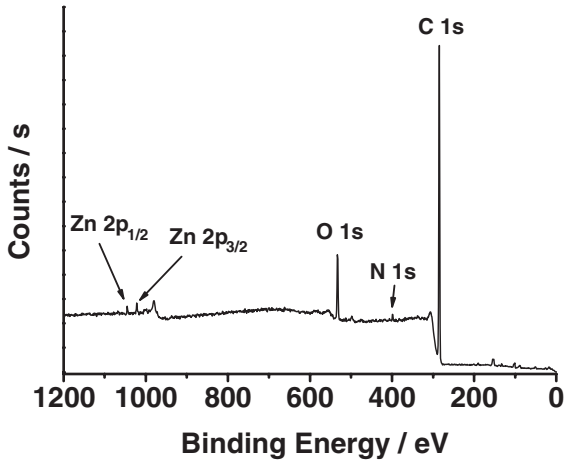

Figure 7. XPS wide-scan spectrum for PDI–POR_4 (**1**).

Waals interactions in this compound. To evaluate the photoelectrochemical performance, we used the OTE/SnO_2/PDI–POR_4 electrode as a working electrode in a photoelectrochemical cell. The photocurrent and photovoltage responses that were recorded following the excitation of the OTE/SnO_2/PDI–POR_4 electrode in the visible light region are shown in Figures 8a and 8b, respectively. The photocurrent response to on/off cycling is prompt, steady, and reproducible during repeated on/off cycles of white light illumination. The short circuit photocurrent density of 1.2 mA cm^{-2} and open circuit voltage of 80 mV were reproducibly obtained during these measurements. The photocurrent stability in the system was rather good during the monitor time, indicating efficient charge transfer took place in this donor–acceptor array. The blank experiments conducted with SnO_2 electrode (i.e., by excluding **1** film) produced no detectable photocurrent under similar experimental conditions.

We also evaluated the power characteristics of the OTE/SnO_2/PDI–POR_4 electrode. Figure 8c shows current–voltage (I–V) characteristics of OTE/SnO_2/PDI–POR_4 under white light illumination (AM 1.5, 100 mW cm^{-2}) and in the dark. The OTE/SnO_2/PDI–POR_4 has a fill factor of 0.42, short circuit current density of 1.2 mA cm^{-2}, open circuit voltage of 80 mV. The power conversion efficiency η of 0.04% was obtained for the device at an input power of 100 mW cm^{-2}. These experiments confirmed the role of PDI–POR_4 array toward harvesting light energy and generating photocurrent during the operation of a photoelectrochemical cell.

To evaluate the response of PDI–POR_4 toward photocurrent generation, the photocurrent action spectra of the OTE/SnO_2/PDI–POR_4 devices is shown in Figure 9. The incident photon-to-photocurrent efficiency (IPCE) values are calculated by normalizing the photocurrent densities for incident light energy and intensity and using the expression

$$\text{IPCE}\ (\%) = 100 \times 1240 \times i/(W_{\text{in}} \times \lambda) \qquad (2)$$

Where i is the photocurrent density (A cm^{-2}), W_{in} is the incident light intensity (W cm^{-2}), and λ is the excitation wavelength (nm). The overall responses of the OTE/SnO_2/PDI–POR_4 devices parallel the broad absorption features (Figure 2), indicating the involvement of the PDI–POR_4 in

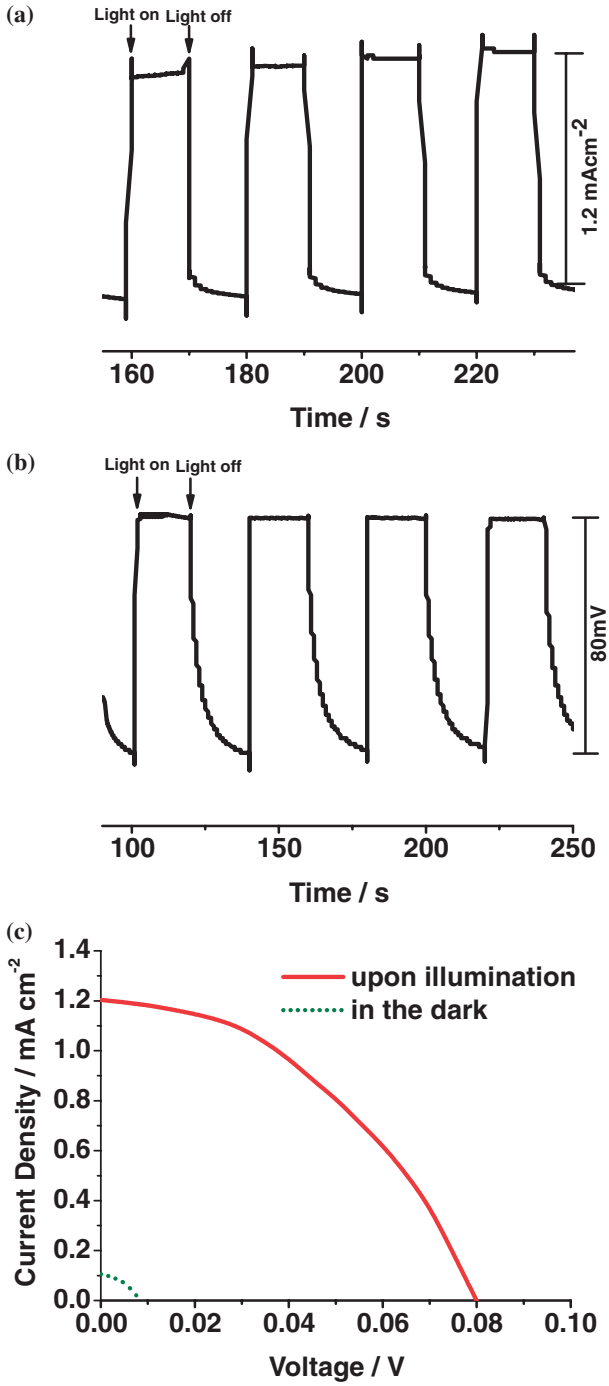

Figure 8. (a) Time dependence of the photocurrent response and (b) photovoltage response of OTE/SnO_2/PDI–POR_4 electrode under white light illumination. (c) *I–V* characteristics of OTE/SnO_2/PDI–POR_4 electrode under AM 1.5 white light illumination (solid lines) and in the dark (dotted lines). Electrolyte, 0.5 M LiI and 0.01 M I_2 in acetonitrile; input power 100 mW cm^{-2}.

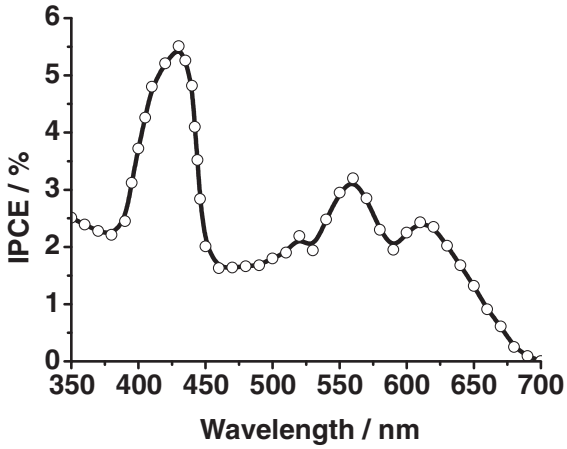

Figure 9. Photocurrent action spectra of OTE/SnO_2/PDI–POR_4 electrode. Electrolyte, 0.5 M LiI and 0.01 M I_2 in acetonitrile.

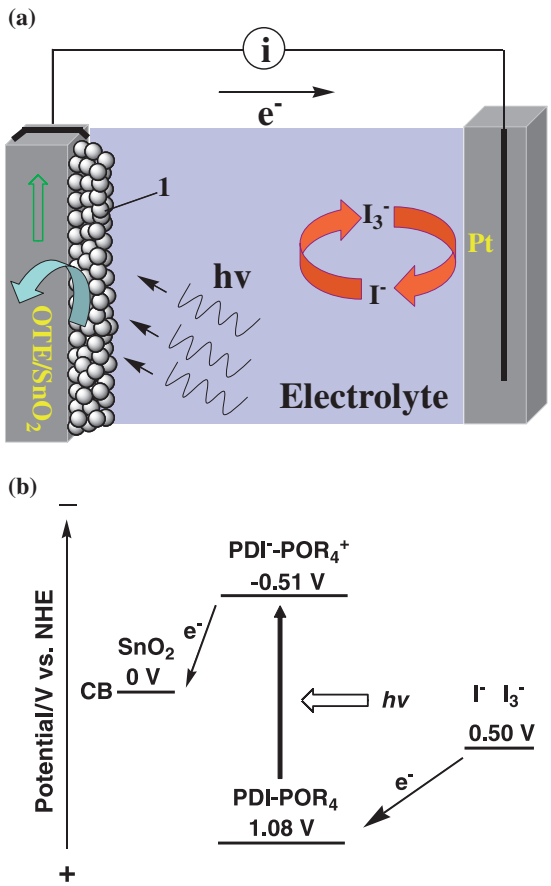

Figure 10. (a) Schematic illustration for photocurrent generation and light-induced charge separation in the photoelectrochemical cell using the OTE/SnO_2/PDI–POR_4 electrode and (b) its energy diagram.

the photocurrent generation. It should be noted here that the IPCE values at 380–450 nm arise from the absorption of the porphyrin moiety, and those at 500–700 nm originate mainly from the absorption of the perylenediimide moiety. In particular, the significant enhancement of the photocurrent generation at around 430 nm and at 560 nm indicates photo-induced electron transfer from the excited singlet state of porphyrin moiety to perylenediimide moiety followed by electron injection from the reduced perylenediimide moiety to the conduction band (CB) of SnO_2.[49,50]

The photocurrent generation trend can be explained using the following mechanism as shown in Figure 10. The levels of

the PDI–POR_4 were determined electrochemically from the first reduction potential and the first oxidation potential of PDI–POR_4 as shown in Table 1. The data are converted to the normal hydrogen electrode (NHE) scale for comparison.[51,52] Taken all together, E(PDI–POR_4) was calculated to be ca. 1.08 V vs. NHE (0.78 V vs. Fc), while E(PDI$^-$–POR_4^+) was ca. −0.51 V vs. NHE (−0.81 V vs. Fc). Assuming that the spherical nanoparticles of array **1** are densely packed on the OTE/SnO_2 surface, upon irradiation, highly efficient electron transfer occurs from the porphyrin (porphyrin moiety in PDI–POR_4 array) excited state. The excited porphyrin component will pass electrons to the perylene component. The reduced perylene component transfers electrons the OTE/SnO_2 electrode and transfers the electron, to produce the current in the circuit. Therefore, in the proposed figure the electron is collected at the electrode surface and the hole is scavenged by the iodide/triiodide couple (I^-/I_3^-) present in the electrolyte system, resulting in the generation of the photocurrent.[53]

Conclusion

In this study, a multichromophore array PDI–POR_4 was synthesized and characterized. This array absorbs strongly from 300 to 700 nm which overlaps the strong radiation scope of sunlight, making it an ideal system to harvest polychromatic light. This significant quenching of the fluorescence suggested that highly efficient photoinduced electron transfer occurs in this array. In toluene, the photoexcited porphyrin unit (POR*) decays very rapidly (lifetime of 0.3 ns) by electron transfer to the perylenediimide moiety, forming PDI$^-$–POR_4^+. By cyclic voltammetry, HOMO and LUMO values of the array were acquired, and these energy values fulfill the energetic conditions required for the proposed electron transfer between the donor and acceptor on excitation of the donor as well as on direct excitation of the acceptor. The morphology of array PDI–POR_4 in polar and nonpolar solvents was investigated with SEM and TEM images, a large quantity of nanospheres with diameters in the range of 50–100 nm was aggregated in different patterns. In methanol, large amounts of spherical nanoparticles are densely packed, whereas ribbon-like structure was observed in nonpolar solvent hexane. The different stacking pattern manifested the solvent effect on the formation of self-assembled structures. The film of the array shows a high capacity to produce rapid and steady photocurrent and photovoltage under the irradiation of white light, this fact confirmed the role of PDI–POR_4 array toward harvesting light energy and generating photocurrent during the operation of a photoelectrochemical cell. The electrode modified with PDI–POR_4 nanospheres exhibited efficient light energy conversion properties, such as a fill factor of 0.42 and a power conversion efficiency (η) of 0.04%. We believe that the present study will provide valuable new information not only for creation of artificial light-harvesting systems but also for the fabrication of photovoltaic devices.

This research was financially supported by (1) National Program on Key Basic Research pre-Projects (pre973) through contract grant number: 2004CCA04800; (2) Scientific Research Foundation for the Returned Overseas Chinese Scholars of State Education Ministry; and (3) Natural Scientific Foundation of Shandong Province (No. 2008ZRB01001). (4) International joint project of Qingdao Bureau of science and technology (No. 10-1-4-97-hz).

Supporting Information

XRD patterns (Figure S1), XPS wide-scan spectra for reference compounds **4** and **7** (Figure S2), high-resolution XPS for **1** (Figure S3), UV–visible absorption spectra of **1** in chloroform solution and in film state (Figure S4), the syntheses and ^{1}H NMR spectrum, FT-IR spectra for array **1** and other compounds are listed in Supporting Information. This material is available free of charge on the web at http://www.csj.jp/journals/bcsj/.

References

1 J. D. Hartgerink, E. Beniash, S. I. Stupp, *Science* **2001**, *294*, 1684.
2 L. Zhi, T. Gorelik, J. Wu, U. Kolb, K. Mullen, *J. Am. Chem. Soc.* **2005**, *127*, 12792.
3 H. A. Zamani, G. Rajabzadeh, M. R. Ganjali, *Bull. Chem. Soc. Jpn.* **2007**, *80*, 172.
4 J. Wang, T. Wågberg, B. Eliasson, L. Edman, *Org. Electron.* **2010**, *11*, 1595.
5 M. J. Ahrens, L. E. Sinks, B. Rybtchinski, W. Liu, B. A. Jones, J. M. Giaimo, A. V. Gusev, A. J. Goshe, D. M. Tiede, M. R. Wasielewski, *J. Am. Chem. Soc.* **2004**, *126*, 8284.
6 A. D. Schwab, D. E. Smith, B. Bond-Watts, D. E. Johnston, J. Hone, A. T. Johnson, J. C. de Paula, W. F. Smith, *Nano Lett.* **2004**, *4*, 1261.
7 S. Zrig, P. Rémy, B. Andrioletti, E. Rose, I. Asselberghs, K. Clays, *J. Org. Chem.* **2008**, *73*, 1563.
8 G. A. Silva, C. Czeisler, K. L. Niece, E. Beniash, D. A. Harrington, J. A. Kessler, S. I. Stupp, *Science* **2004**, *303*, 1352.
9 V. Percec, M. Glodde, T. K. Bera, Y. Miura, I. Shiyanovskaya, K. D. Singer, V. S. K. Balagurusamy, P. A. Heiney, I. Schnell, A. Rapp, H.-W. Spiess, S. D. Hudson, H. Duan, *Nature* **2002**, *417*, 384.
10 T. Yokoyama, S. Yokoyama, T. Kamikado, Y. Okuno, S. Mashiko, *Nature* **2001**, *413*, 619.
11 T. Ishi-i, K. Murakami, Y. Imai, S. Mataka, *Org. Lett.* **2005**, *7*, 3175.
12 Y.-W. Zhong, Y. Matsuo, E. Nakamura, *J. Am. Chem. Soc.* **2007**, *129*, 3052.
13 C.-Z. Li, Y. Matsuo, E. Nakamura, *J. Am. Chem. Soc.* **2009**, *131*, 17058.
14 H. Imahori, S. Fukuzumi, *Adv. Funct. Mater.* **2004**, *14*, 525.
15 S. Eu, S. Hayashi, T. Umeyama, A. Oguro, M. Kawasaki, N. Kadota, Y. Matano, H. Imahori, *J. Phys. Chem. C* **2007**, *111*, 3528.
16 S. Tanaka, M. Shirakawa, K. Kaneko, M. Takeuchi, S. Shinkai, *Langmuir* **2005**, *21*, 2163.
17 C. Luo, D. M. Guldi, H. Imahori, K. Tamaki, Y. Sakata, *J. Am. Chem. Soc.* **2000**, *122*, 6535.
18 P. A. Liddell, G. Kodis, A. L. Moore, T. A. Moore, D. Gust, *J. Am. Chem. Soc.* **2002**, *124*, 7668.
19 M. D. Yilmaz, O. A. Bozdemir, E. U. Akkaya, *Org. Lett.* **2006**, *8*, 2871.
20 J. M. Serin, D. W. Brousmiche, J. M. J. Fréchet, *Chem. Commun.* **2002**, 2605.
21 Z. Zhou, J. L. Brusso, S. Holdcroft, *Chem. Mater.* **2010**, *22*, 2287.

22 X. Li, L. E. Sinks, B. Rybtchinski, M. R. Wasielewski, *J. Am. Chem. Soc.* **2004**, *126*, 10810.
23 K. Vasseur, C. Rolin, S. Vandezande, K. Temst, L. Froyen, P. Heremans, *J. Phys. Chem. C* **2010**, *114*, 2730.
24 Y. Chen, Y. Lin, M. E. El-Khouly, X. Zhuang, Y. Araki, O. Ito, W. Zhang, *J. Phys. Chem. C* **2007**, *111*, 16096.
25 R. F. Kelley, M. J. Tauber, M. R. Wasielewski, *J. Am. Chem. Soc.* **2006**, *128*, 4779.
26 P. M. Kazmaier, R. Hoffmann, *J. Am. Chem. Soc.* **1994**, *116*, 9684.
27 C. Hippius, F. Schlosser, M. O. Vysotsky, V. Böhmer, F. Würthner, *J. Am. Chem. Soc.* **2006**, *128*, 3870.
28 P. Bauer, H. Wietasch, S. M. Lindner, M. Thelakkat, *Chem. Mater.* **2007**, *19*, 88.
29 T. van der Boom, R. T. Hayes, Y. Zhao, P. J. Bushard, E. A. Weiss, M. R. Wasielewski, *J. Am. Chem. Soc.* **2002**, *124*, 9582.
30 A. Prodi, C. Chiorboli, F. Scandola, E. Iengo, E. Alessio, R. Dobrawa, F. Würthner, *J. Am. Chem. Soc.* **2005**, *127*, 1454.
31 S. Xiao, M. E. El-Khouly, Y. Li, Z. Gan, H. Liu, L. Jiang, Y. Araki, O. Ito, D. Zhu, *J. Phys. Chem. B* **2005**, *109*, 3658.
32 J. S. Lindsey, R. W. Wagner, *J. Org. Chem.* **1989**, *54*, 828.
33 M. Thelakkat, H.-W. Schmidt, *Adv. Mater.* **1998**, *10*, 219.
34 F. Würthner, Z. Chen, V. Dehm, V. Stepanenko, *Chem. Commun.* **2006**, 1188.
35 T. Ezuhara, K. Endo, Y. Aoyama, *J. Am. Chem. Soc.* **1999**, *121*, 3279.
36 S. R. Greenfield, W. A. Svec, D. Gosztola, M. R. Wasielewski, *J. Am. Chem. Soc.* **1996**, *118*, 6767.
37 R. F. Kelley, W. S. Shin, B. Rybtchinski, L. E. Sinks, M. R. Wasielewski, *J. Am. Chem. Soc.* **2007**, *129*, 3173.
38 R. Gómez, J. L. Segura, N. Martín, *Org. Lett.* **2005**, *7*, 717.
39 Y. Liu, N. Wang, Y. Li, H. Liu, Y. Li, J. Xiao, X. Xu, C. Huang, S. Cui, D. Zhu, *Macromolecules* **2005**, *38*, 4880.
40 G. D. Scholes, K. P. Ghiggino, A. M. Oliver, M. N. Paddon-Row, *J. Am. Chem. Soc.* **1993**, *115*, 4345.
41 Y. Cakmak, E. U. Akkaya, *Org. Lett.* **2009**, *11*, 85.
42 J. Hernando, M. van der Schaaf, E. M. H. P. van Dijk, M. Sauer, M. F. García-Parajó, N. F. van Hulst, *J. Phys. Chem. A* **2003**, *107*, 43.
43 A. Fürstenberg, E. Vauthey, *J. Phys. Chem. B* **2007**, *111*, 12610.
44 M. Srinivasarao, D. Collings, A. Philips, S. Patel, *Science* **2001**, *292*, 79.
45 Y. Gao, X. Zhang, C. Ma, X. Li, J. Jiang, *J. Am. Chem. Soc.* **2008**, *130*, 17044.
46 G. A. Rajkumar, A. S. D. Sandanayaka, K. Ikeshita, M. Itou, Y. Araki, Y. Furusho, N. Kihara, O. Ito, T. Takata, *J. Phys. Chem. A* **2005**, *109*, 2428.
47 M. S. Killian, J.-F. Gnichwitz, A. Hirsch, P. Schmuki, J. Kunze, *Langmuir* **2010**, *26*, 3531.
48 K. Akatsuka, Y. Ebina, M. Muramatsu, T. Sato, H. Hester, D. Kumaresan, R. H. Schmehl, T. Sasaki, M. Haga, *Langmuir* **2007**, *23*, 6730.
49 T. Hasobe, S. Fukuzumi, P. V. Kamat, *J. Phys. Chem. B* **2006**, *110*, 25477.
50 A. Kira, T. Umeyama, Y. Matano, K. Yoshida, S. Isoda, M. Isosomppi, N. V. Tkachenko, H. Lemmetyinen, H. Imahori, *Langmuir* **2006**, *22*, 5497.
51 W. B. Heuer, H.-L. Xia, M. Abrahamsson, Z. Zhou, S. Ardo, A. A. N. Sarjeant, G. J. Meyer, *Inorg. Chem.* **2010**, *49*, 7726.
52 A. Kira, T. Umeyama, Y. Matano, K. Yoshida, S. Isoda, J. K. Park, D. Kim, H. Imahori, *J. Am. Chem. Soc.* **2009**, *131*, 3198.
53 H. Imahori, T. Umeyama, *J. Phys. Chem. C* **2009**, *113*, 9029.